Chaos

A normal form method for the determination of oscillations characteristics near the primary Hopf bifurcation in bandpass optoelectronic oscillators: Theory and experiment

Cite as: Chaos **29**, 033104 (2019); https://doi.org/10.1063/1.5064679
Submitted: 07 October 2018 . Accepted: 08 February 2019 . Published Online: 01 March 2019

Jimmi H. Talla Mbé, Paul Woafo, and Yanne K. Chembo

View Online Export Citation CrossMark

ARTICLES YOU MAY BE INTERESTED IN

Mixed mode oscillations and phase locking in coupled FitzHugh-Nagumo model neurons
Chaos: An Interdisciplinary Journal of Nonlinear Science **29**, 033105 (2019); https://doi.org/10.1063/1.5050178

Critical behavior of power transmission network complex dynamics in the OPA model
Chaos: An Interdisciplinary Journal of Nonlinear Science **29**, 033103 (2019); https://doi.org/10.1063/1.5066370

Nonlinear dynamics with Hopf bifurcations by targeted mutation in the system of rock-paper-scissors metaphor
Chaos: An Interdisciplinary Journal of Nonlinear Science **29**, 033102 (2019); https://doi.org/10.1063/1.5081966

AIP Publishing

© 2019 Author(s).

A normal form method for the determination of oscillations characteristics near the primary Hopf bifurcation in bandpass optoelectronic oscillators: Theory and experiment

Cite as: Chaos **29**, 033104 (2019); doi: 10.1063/1.5064679
Submitted: 7 October 2018 · Accepted: 8 February 2019 ·
Published Online: 1 March 2019

View Online Export Citation CrossMark

Jimmi H. Talla Mbé,[1,2,a)] Paul Woafo,[2,3] and Yanne K. Chembo[4,b)]

AFFILIATIONS

[1]Laboratory of Condensed Matter, Electronics and Signal Processing, Department of Physics, University of Dschang, P.O. Box 67, Dschang, Cameroon
[2]Laboratory of Modelling and Simulation in Engineering, Biomimetics and Prototypes, Department of Physics, Faculty of Science, University of Yaoundé 1, P.O. Box 812, Yaoundé, Cameroon
[3]Applied Physics Research Group (APHY), Vrije Universiteit Brussel, Pleinlaan 2, 1050 Brussels, Belgium
[4]GeorgiaTech-CNRS Joint International Laboratory (UMI 2958), Atlanta Mirror Site, School of Electrical and Computer Engineering, 777 Atlantic Dr NW, Atlanta, Georgia 30332, USA

[a)]**Electronic mail:** jhtallam@yahoo.fr
[b)]**Present address:** Institute for Research in Electronics and Applied Physics (IREAP) and Department of Electrical and Computer Engineering, University of Maryland, College Park, Maryland 20742, USA.

ABSTRACT

We propose a framework for the analysis of the integro-differential delay Ikeda equations ruling the dynamics of bandpass optoelectronic oscillators (OEOs). Our framework is based on the normal form reduction of OEOs and helps in the determination of the amplitude and the frequency of the primary Hopf limit-cycles as a function of the time delay and other parameters. The study is carried for both the negative and the positive slopes of the sinusoidal transfer function, and our analytical results are confirmed by the numerical and experimental data.

Published under license by AIP Publishing. https://doi.org/10.1063/1.5064679

Owing to the richness of their dynamical behavior, OEOs have found many applications such as ultra-stable microwave generation, optical communications, and neuromorphic computing, amongst others. This richness results from the complex interplay between the system parameters, namely, the two timescales of the bandpass filter, the time delay, the feedback loop strength, and the nonlinear transfer function. The aim of this work is to analytically compute and experimentally validate the expressions of the frequency and the amplitude of the primary Hopf limit-cycles as a function of the parameters mentioned above, without neglecting the time delay as it is usually the case. Since primary Hopf limit-cycles are important attractors for most of the applications related to these oscillators, such analytical expressions help for the better calibration and optimization of OEOs.

I. INTRODUCTION

Time delay effects appear naturally in various physical, biological, chemical, and technological systems and are sources of oscillatory instabilities.[1,2] Delay differential systems are indeed ubiquitous, as they emerged in a wide variety of fundamental and applied disciplinary area such as electronics, fluid dynamics, biological models, chemistry, and photonics.[3–9] In recent years, one of the most popular benchmarks to study nonlinear delay dynamics has been the optoelectronic oscillator (OEO), as comprehensively reviewed in Ref. 10. OEOs have found numerous practical applications in areas as diverse as microwave generation,[11–22] chaos-based communications,[23–27] chaotic radars,[28] bioinspired information processing,[29] or sensing.[30]

Published under license by AIP Publishing.

The dynamics of OEOs can generally be investigated using the paradigm of the Ikeda equation.[31] Indeed, in the case the feedback loop features a wide bandpass filtering characteristic (bandwidth much larger than the free-spectral range), the system can display a rich dynamics that include limit-cycles, pulse packages, chaotic breathers, and hyperchaos.[32–43] The richness of the bandpass OEO dynamics originates from the interplay between its three main timescales, related to the delay and to the high- and low-pass filter timescales. In particular, the primary Hopf bifurcation as the feedback gain is increased has evidenced several scenarios, characterized by oscillation frequencies that are split by several orders of magnitude.[32,34,35,39]

The analytic study of these attractors is generally difficult to carry out, mainly because time-delayed systems are inherently infinite-dimensional. However, close to bifurcation points, the theoretical analysis of delayed systems can be performed by circumscribing their long-term dynamics in an invariant manifold where their most significant dynamical signatures can be recovered. This is essentially the main idea underlying the technique of normal form reduction.[44–49]

In this paper, we develop this normal form approach for the characterization of the integro-differential delay systems, near the primary Hopf bifurcation. The paper is organized as follows. In Sec. II, the system is presented along with its mathematical model. Section III is devoted to the bifurcation analysis of the oscillator, which is then used in Sec. IV to perform the normal form analysis, which helps one to understand the oscillation properties of the system. Section V concludes the article.

II. THE SYSTEM

The system under study is displayed in Fig. 1. It consists of a telecommunication continuous-wave laser diode ($\lambda_L \simeq 1550$ nm), which sends a polarization-controlled signal via a polarization controller (PC) to an integrated electro-optic Mach-Zehnder intensity modulator (MZM) of half-wave voltages $V_{\pi dc} = 5$ V and $V_{\pi rf} = 3.8$ V. The modulated light at the output of the MZM is delayed using an optical fiber spool (DL) with a time delay equal to $T = 60$ ns, before being converted to an electrical signal with a photodiode (PD) of responsivity S. The resulting electrical signal is then filtered with a wide bandpass filter. The output signal of the filter is amplified using a RF amplifier (Amp). At the output of the amplifier, a microwave coupler (MC) is used to split the electrical power into two: One part is re-injected into the RF input of the MZM, thereby closing the loop of the oscillator; the other part is used to monitor the signal of the oscillator using a digital oscilloscope. This OEO then can be described by the following Ikeda integro-differential delay equation (iDDE):[32]

$$x + \tau\frac{dx}{dt} + \frac{1}{\theta}\int_{t_0}^{t} x(s)ds = \beta\cos^2[x_T + \phi], \tag{1}$$

where $x = \pi V/2V_{\pi rf}$ is the dimensionless variable standing for the voltage V(t) at the radio-frequency (RF) input of the MZM and $x_T \equiv x(t-T)$ is the time-delayed variable, while the parameters of the equation are the high cut-off time $\tau = 1/2\pi f_H$ and the low cut-off time $\theta = 1/2\pi f_L$ of the bandpass filter. Throughout this article, the cut-off times of the bandpass filter are $\theta = 16.24$ μs and $\tau = 1.06$ ns. The normalized loop-gain is $\beta = \pi S\varepsilon P/2V_{\pi rf}$, where P is the laser pump and ε is the overall attenuation of the feedback loop. The offset phase $\phi = \pi V_B/2V_{\pi dc}$ defined the slope of the nonlinear transfer component, with V_B being a constant bias voltage.

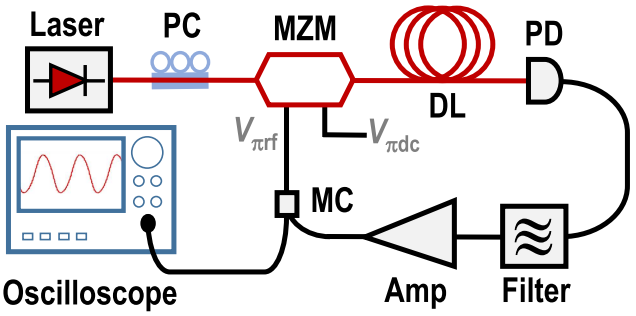

FIG. 1. Experimental setup of the OEO. PC, polarization controller; MZM, Mach-Zehnder modulator; DL, delay line; PD, photodiode; Amp, RF amplification; MC, microwave coupler.

The parameters β and T are the two independent control parameters for the system, and the purpose of this paper is to gain insight into the bifurcation dynamics of the oscillator as a function of these two parameters.

III. BIFURCATION ANALYSIS OF THE OEO

Our first step is to rescale Eq. (1) with regard to the dimensionless time t/τ, which we will still refer to as t for the sake of mathematical convenience. This equation can then be rewritten under the following normalized form:

$$\frac{dx_1}{dt} = -x_1 - \sigma x_2 + \beta[\cos^2(x_{1\nu} + \phi) - \cos^2\phi], \tag{2}$$

$$\frac{dx_2}{dt} = x_1, \tag{3}$$

with $x_1 \equiv x$ and $x_2(t) \equiv \frac{1}{\tau}\int_0^t x(s)\,ds$. The parameter $\sigma = \tau/\theta$ is the ratio between the low and high cut-off frequencies, and $\nu = T/\tau$ represents the normalized delay.

In order to derive the normal form, it is convenient to separate Eqs. (2) and (3) into a linear and nonlinear part. One should note that just before the Hopf bifurcation point, the whole dynamics of the system is ruled by the trivial stable equilibrium point $(x_{1,0}, x_{2,0}) = (0,0)$, and this trivial fixed point might lose its stability via a Hopf bifurcation. Therefore, in the neighborhood of the Hopf bifurcation point, a Taylor

Published under license by AIP Publishing.

expansion around that equilibrium can be performed as

$$\frac{dx_1}{dt} = -x_1 - \sigma x_2 - \beta\left[\sin(2\phi)x_{1\nu} + \cos(2\phi)x_{1\nu}^2 - \frac{2}{3}\sin(2\phi)x_{1\nu}^3\right], \tag{4}$$

$$\frac{dx_2}{dt} = x_1. \tag{5}$$

For mathematical simplicity and without loss of generality, Eqs. (4) and (5) are rewritten under the matrix form

$$\frac{dX}{dt} = LX + RX_\nu + F(X_\nu), \tag{6}$$

with $X = (x_1, x_2)^T$, where the superscript T stands for the transpose. This equation is characterized by the matrices

$$L = \begin{bmatrix} -1 & -\sigma \\ 1 & 0 \end{bmatrix} \quad \text{and} \quad R = \gamma \begin{bmatrix} 1 & 0 \\ 0 & 0 \end{bmatrix}, \tag{7}$$

with $\gamma = \beta\sin(2\phi)$ being the effective linearized gain and by the column vector $F(X_\nu) = \beta[-\cos(2\phi)x_{1\nu}^2 + (2/3)\sin(2\phi)x_{1\nu}^3, 0]^T$.

It is important to verify that the truncated flow [Eqs. (4) and (5)] provides an accurate description of the OEO dynamics close to the Hopf bifurcation point and agrees with the results obtained directly from the original flow [Eqs. (2) and (3)]. Figure 2(b) confirms that the truncated flow is indeed a valid approximation that can be used later on for the normal form analysis.

We consider that the linear part

$$\frac{dX}{dt} = LX + RX_\nu \tag{8}$$

of Eq. (6) has solutions that can be written under the form $X = X_0 e^{\lambda t}$. The eigenvalue $\lambda = \eta + i\omega$ verifies the following equation:

$$\lambda[1 + \lambda + \gamma e^{-\lambda\nu}] + \sigma = 0 \tag{9}$$

and the solutions are asymptotically stable when $\eta < 0$ and unstable when $\eta > 0$, while the critical case $\eta = 0$ marks the Hopf bifurcation point. When the critical case is satisfied, the values of the effective gain $\gamma = \gamma_c = \beta_c\sin(2\phi)$ and frequency $\omega = \omega_c$ fulfill accordingly

$$-\omega_c^2 + \gamma_c\omega_c\sin(\omega_c\nu) + \sigma = 0, \tag{10}$$

$$\omega_c + \gamma_c\omega_c\cos(\omega_c\nu) = 0. \tag{11}$$

Combining Eqs. (10) and (11), the critical frequency verifies the transcendental equation

$$\sigma - \omega_c^2 = \omega_c\tan(\omega_c\nu). \tag{12}$$

It should be noted that we have $\nu \neq 0$ and $\sigma \neq \omega_c^2$, and it is known that solving Eqs. (10)–(12) yields two different Hopf bifurcations.[32] For the negative slope case ($\gamma < 0$), we obtain

$$\gamma_{c,n} \simeq -1 - \frac{T}{2\theta} \simeq -1 - \frac{\sigma\nu}{2}, \tag{13}$$

$$\omega_{c,n} \simeq \tau\sqrt{\frac{1}{\theta T}} \simeq \sqrt{\frac{\sigma}{\nu}}, \tag{14}$$

which correspond to slow-scale oscillations, while for the positive slope case ($\gamma > 0$), we have

$$\gamma_{c,p} \simeq 1 + \frac{1}{2}\left(\frac{\sigma\nu^2 - \pi^2}{\pi\nu}\right)^2, \tag{15}$$

$$\omega_{c,p} \simeq \pi\frac{\tau}{T} \simeq \frac{\pi}{\nu} \tag{16}$$

corresponding to fast-scale oscillations. Note that throughout the article, the subscripts n and p refer to the negative and positive slopes, respectively.

The study of the linearized flow provides insight into the dynamics of the system in the close neighborhood of the bifurcation but gives little information about what happens beyond. Such an insight can be achieved using the normal form of the system, as developed in Sec. IV.

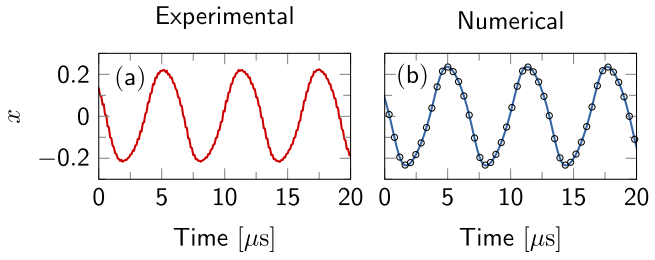

FIG. 2. Timetraces of the limit-cycle near the Hopf bifurcation point, with $\phi = -\pi/4$. (a) Experimental timetrace with $P = 8.4$ mW, $V_B = 13.22$ V. (b) Numerical timetrace, with parameters $\beta = 1.03$, $\phi = -0.795$, $\nu = 56.6$, and $\sigma = 6.53 \times 10^{-5}$. The solid line represents the timetrace obtained with Eqs. (2) and (3), while the symbols (black circles) correspond to the numerical results obtained with Eqs. (4) and (5). For the numerical simulations, the initial condition has been uniformly set to $x_1 = 0.2$ for the time interval $[-\nu, 0]$ and $x_2 = 10^{-3}$ at $t = 0$.

IV. DERIVATION OF THE NORMAL FORM THROUGH THE METHOD OF CENTER MANIFOLD REDUCTION

There exist different methods for the computation of the normal form for a dynamical system (see, for example, Refs. 46–48). In this article, we choose to follow the method of center manifold reduction,[48] which is convenient, based on the fact that the long-time dynamics of a system can be reduced to the dynamics on its center manifold, also known as the *reduced form* of the system, or simply its *normal form*. This method is appropriate for our system since no small quantity multiplies the right hand of Eq. (2); otherwise, the method of multiple time scales would have been used. Moreover, the method of center manifold reduction has already been successfully applied and tested on other delay systems.[48,49] The reader can refer to these references for more details on the computational details, in particular those related to Eqs. (18)–(34).

Let us introduce the bifurcation parameter $\delta = \gamma - \gamma_c = (\beta - \beta_c)\sin(2\phi)$, which represents the relative gain, and is

Published under license by AIP Publishing.

such that $\delta \ll 1$ near the Hopf bifurcation point. For a negative slope, $\delta < 0$, whereas $\delta > 0$ for the positive slope. By Taylor-expanding Eq. (6) with respect to δ and neglecting higher-order terms, it yields

$$\frac{dX}{dt} = \mathsf{L}X + \mathsf{R}_c X_\nu + \mathsf{F}(X_\nu), \tag{17}$$

where R_c is the operator R evaluated at the critical Hopf bifurcation point. The vector $\mathsf{F}(X_\nu)$ is a third-order polynomial function defined as $\mathsf{F}(X_\nu) = (-\delta x_{1\nu} - \gamma_c \zeta x_{1\nu}^2 + \frac{2}{3}\gamma_c x_{1\nu}^3, 0)^T$, with $\zeta = [\tan(2\phi)]^{-1}$. Equation (17) is a delay-differential equation, and the evaluation of the corresponding variable requires to take into account the state of the system within two time intervals $[-\nu, 0]$ and $[0, +\infty]$. It is convenient to separate the times in the two intervals. Let us call the time μ within the interval $[-\nu, 0]$ and maintain the notation of time t within $[0, +\infty]$. By so doing, Eq. (17) becomes a step function

$$\frac{dX_t(\mu)}{dt} = \mathsf{A}X_t(\mu) + \mathsf{G}[X_t(\mu)], \tag{18}$$

where $X_t(\mu) = X(t + \mu)$ is a portion of the solution trajectory in the recent past. A is the linear operator with pure imaginary eigenvalue $i\omega_c$, which transforms a center subspace function $p(\mu)$ as follows:

$$\begin{aligned} \mathsf{A}p(\mu) &= i\omega_c p(\mu) \\ &= \begin{cases} \dfrac{dp(\mu)}{d\mu} & \text{for } -\nu \le \mu \le 0, \\ \mathsf{L}p(0) + \mathsf{R}_c p(-\nu) & \text{for } \mu = 0. \end{cases} \end{aligned} \tag{19}$$

Since the eigenvalues for the Hopf bifurcation point are symmetric ($\pm i\omega_c$), it is advisable to define the adjoint operator A^* of A with the eigenvalue equal to the conjugate of the first one and which applied on another given subspace function $q(\mu)$ yields

$$\begin{aligned} \mathsf{A}^* q(\mu) &= -i\omega_c q(\mu) \\ &= \begin{cases} -\dfrac{dq(\mu)}{d\mu} & \text{for } 0 \le \mu \le \nu, \\ \mathsf{L}^* q(0) + \mathsf{R}_c^* q(\nu) & \text{for } \mu = 0, \end{cases} \end{aligned} \tag{20}$$

where L^* and R_c^* are the adjoints of the operators L and R_c, respectively. In Eq. (18), the vector function G is deduced from Eq. (17) as

$$\mathsf{G} = \begin{cases} 0 & \text{for } -\nu \le \mu \le 0, \\ \mathsf{F} & \text{for } \mu = 0. \end{cases} \tag{21}$$

One key condition in the theory of the center manifold reduction requires that the functions p and q obey the inner product

$$\langle q, p \rangle = \bar{q}(0)p(0) + \int_{-\nu}^{0} \bar{q}(\xi + \nu)\mathsf{R}_c^* p(\xi) d\xi, \tag{22}$$

with overline expressing complex conjugation. Since $X_t(\mu)$ must be finite, it is necessary to introduce a normalization condition such that $\langle q, p \rangle = 1$ and $\langle q, \bar{p} \rangle = 0$.

Using the inner product defined in Eq. (22), the solutions of Eqs. (19) and (20) are, respectively,

$$p(\mu) = \begin{pmatrix} i\omega_c \\ 1 \end{pmatrix} e^{i\omega_c \mu}; \quad q(\mu) = b \begin{pmatrix} 1 \\ -i\sigma/\omega_c \end{pmatrix} e^{i\omega_c \mu}, \tag{23}$$

with

$$b = \left[1 - 2i\omega_c + \gamma_c(1 + i\omega_c \nu)e^{i\omega_c \mu}\right]^{-1} \tag{24}$$

being a complex-valued parameter.

Having determined the center subspace $p(\mu)$ and its adjoint $q(\mu)$, the following step consists of decomposing $X_t(\mu)$ into two components: the first one is $y(t)p(\mu) + \bar{y}(t)\bar{p}(\mu)$, and it lies in the center subspace; the second one is the infinite-dimensional component $u_t(\mu)$, which is transverse to the center subspace. We can therefore write

$$X_t(\mu) = y(t)p(\mu) + \bar{y}(t)\bar{p}(\mu) + u_t(\mu) \tag{25}$$

and the transversality of $u_t(\mu)$ yields: $\langle p, u \rangle = 0$ and $\langle \bar{p}, u \rangle = 0$. Then, by substituting Eq. (25) into Eq. (18) and using the inner products, we find that $y(t)$ satisfies the following first-order differential equation:

$$\begin{aligned} \dot{y}(t) = {} & i\omega_c y - \delta\, \bar{b}\rho y - \bar{b}\gamma_c \zeta(\rho y + \bar{\rho}\,\bar{y})^2 \\ & - 2i\,\bar{b}\gamma_c^2 \zeta^2 \rho^2 \bar{\rho} \left[\frac{\bar{b}}{\omega_c}\rho - 7\frac{b}{3\omega_c}\rho + 2\omega_c \Gamma e^{-2i\omega_c \nu} \right] y^2 \bar{y} \\ & + 2\bar{b}\gamma_c \rho^2 \bar{\rho} y^2 \bar{y} + \text{NRT}. \end{aligned} \tag{26}$$

The acronym NRT represents the *non-resonant terms* of the equation, and the overdot stands for differentiation with respect to time. The complex coefficients ρ and Γ are explicitly given by

$$\rho = i\omega_c e^{-i\omega_c \nu}, \tag{27}$$

$$\Gamma = \left[4\omega_c^2 - \sigma - 2i\omega_c\left(1 + \gamma_c e^{-2i\omega_c \nu}\right)\right]^{-1}. \tag{28}$$

Finally, the last step is to perform the near-identity transformation, with respect to Eq. (26), which is as follows:[48]

$$y(t) = z(t) + d_1 z^2(t) + d_2 z(t)\bar{z}(t) + d_3 \bar{z}^2(t). \tag{29}$$

By replacing Eq. (29) into Eq. (26) and eliminating the secular terms, the coefficients d_j $(j = 1, 2, 3)$ yield

$$d_1 = \frac{i\bar{b}\gamma_c \zeta}{\omega_c}\rho^2, \tag{30}$$

$$d_2 = -\frac{2i\bar{b}\gamma_c \zeta}{\omega_c}\rho\bar{\rho}, \tag{31}$$

$$d_3 = -\frac{i\bar{b}\gamma_c \zeta}{3\omega_c}\bar{\rho}^2. \tag{32}$$

The remaining terms, which are non-secular, constituting the complex normal form of the system are given by

$$\dot{z} = i\omega_c z - \delta\,\bar{b}\rho z + \bar{b}\gamma_c \rho^2 \bar{\rho}\left[2 - 4i\omega_c \gamma_c \zeta^2 \Gamma e^{-2i\omega_c \nu}\right] z^2 \bar{z} \tag{33}$$

so that the local dynamics of Eq. (1) is ruled by Eq. (33). In the first approximation, the solution of Eq. (33) can be expressed

Published under license by AIP Publishing.

as $z(t) = \mathcal{A}(t)e^{i\omega_c t}$. Hence, the complex amplitude $\mathcal{A}$ fulfills the following first order differential equation, which is its complex normal form:

$$\dot{\mathcal{A}} = -\delta\,\Lambda_1\mathcal{A} + \Lambda_2\mathcal{A}^2\overline{\mathcal{A}}. \tag{34}$$

The coefficients Λ_1 and Λ_2 have the following expressions:

$$\Lambda_1 = \frac{i\omega_c e^{-i\omega_c\nu}}{1+2i\omega_c+\gamma_c(1-i\omega_c\nu)e^{-i\omega_c\nu}}, \tag{35}$$

$$\Lambda_2 = 2\gamma_c\omega_c^2\Lambda_1\left[1-2i\omega_c\gamma_c\zeta^2\Gamma e^{-2i\omega_c\nu}\right]. \tag{36}$$

Equation (34) is a complex equation, which can furthermore be decomposed using $\mathcal{A} = \mathrm{A}(t)\,e^{i\varphi(t)}$ and this enabling to track the amplitude and phase dynamics around the bifurcation.

Beyond the Hopf bifurcation point at the gain value $|\gamma_c|$, the system undergoes a Hopf bifurcation, and from Eq. (34), it can be shown that the frequency and amplitude of the limit-cycle can be explicitly defined as a function of $\delta \equiv \gamma - \gamma_c$ following

$$\omega_{\text{eff}} = \omega_c + (\gamma-\gamma_c)\,\frac{\Re[\Lambda_1]\Im[\Lambda_2]-\Im[\Lambda_1]\Re[\Lambda_2]}{\{\Re[\Lambda_2]\}^2}, \tag{37}$$

$$\mathrm{A} = 2\omega_c\sqrt{(\gamma-\gamma_c)\,\frac{\Re[\Lambda_1]}{\Re[\Lambda_2]}}. \tag{38}$$

The symbols $\Re$ and $\Im$ stand for the real and the imaginary parts of their arguments, respectively. The above formulas lead to drastically different behaviors depending on the actual sign of γ_c [or equivalently, the sign of $\sin(2\phi)$]. It is noteworthy that in the particular case where $\gamma_c < 0$ with $\phi = -\pi/4$, the amplitude can be simplified as

$$\mathrm{A} \simeq \sqrt{-2\,\frac{\beta-\beta_c}{1+\frac{\sigma\nu}{2}}}, \tag{39}$$

while it can be approximated as

$$\mathrm{A} \simeq \sqrt{2\,\frac{\beta-\beta_c}{1+\frac{1}{2}\left(\frac{\sigma\nu^2-\pi^2}{\pi\nu}\right)^2}} \tag{40}$$

in the case where $\gamma_c > 0$ with $\phi = \pi/4$. Figure 3 displays an example of plots of the variations of amplitude when the gain is increased beyond the Hopf bifurcation point, for positive and negative γ_c, with a very good agreement between numerical and analytical results. Indeed, it is known that the amplitude is expected to scale as $\sqrt{|\delta|}$ beyond the Hopf bifurcation, but a key challenge in the case of a delayed system is to be able to compute the proportionality factor as a function of all the time constants of the oscillator. On the other hand, Fig. 4 shows the variations of the oscillation frequency as a function of the normalized time delay. Here again, the agreement between theory and numerical simulations is excellent and validates the normal form analysis. It is noteworthy that the oscillation frequency monotonously decreases as the time delay increases. This trend is accurately described by the normal form analysis even in the asymptotic case of very large delays ($\nu > 1000$), even though the limit-cycles have significantly different characteristic frequencies.

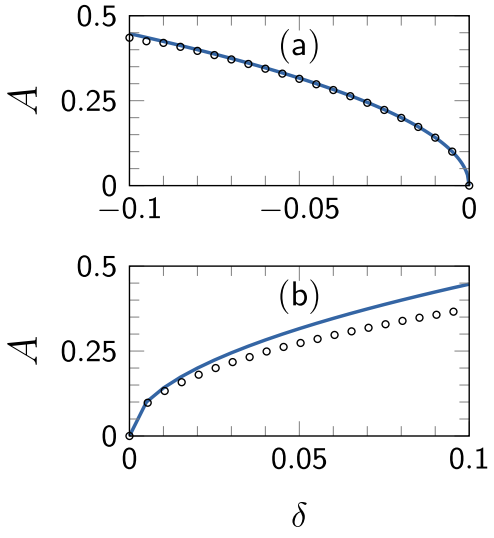

FIG. 3. Variation of the limit-cycle amplitude as the gain is varied beyond the Hopf bifurcation point γ_c as $\delta \equiv \gamma - \gamma_c$. The analytical results obtained from Eq. (38) are displayed with a solid line, while the numerical results obtained using Eqs. (2) and (3) are represented with the symbols (black circles). (a) Case of negative slope with $\phi = -\pi/4$; (b) case of positive slope with $\phi = \pi/4$. Both curves are almost symmetric to zero, confirming that the negative slope is only defined for $\delta < 0$ and the positive slope requires $\delta > 0$.

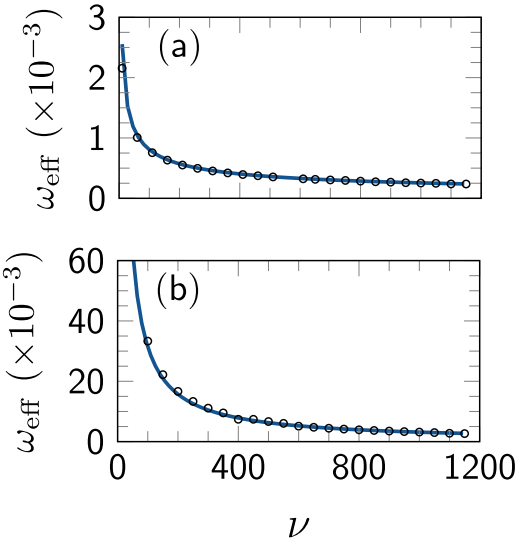

FIG. 4. Evolution of the limit-cycle frequency as a function of the normalized delay $\nu = T/\tau$. The analytical results obtained from Eq. (37) are displayed with a solid line, while the numerical results obtained using Eqs. (2) and (3) are represented with the symbols (black circles). (a) Case of negative slope with $\phi = -\pi/4$ and $\delta = -4 \times 10^{-2}$ and (b) case of positive slope with $\phi = \pi/4$ and $\delta = 1.5 \times 10^{-2}$.

Published under license by AIP Publishing.

V. CONCLUSION

In this work, we have computed the normal form of the Ikeda integro-differential delay equation, which rules the dynamics of bandpass optoelectronic oscillators. These normal forms have allowed us to evaluate the frequency and the amplitude of the Hopf-induced limit-cycles, as a function of system parameters such as the gain, the filter time-constants, and the delay. Unlike the typical case of limit-cycles in systems without delay, normal forms in delayed oscillators have to account for the dependence of the amplitude and oscillation frequency with regard to the delay. The technique we have used in this work permitted us to evaluate this dependency with great accuracy and over a wide range of parameters.

In future research, we intend to explore the normal forms of other architectures of OEOs (such as Refs. 50 and 51), and in general, of different types of time-delayed systems.[1,2,48] We also aim to develop asymptotic techniques to deal with the cases of very long[10,14] or very short[28] time delays and experimentally investigate the effect of a large variation of these time delays.[52]

ACKNOWLEDGMENTS

J.H.T.M. acknowledges the financial support from AGNES (African-German Network of Excellence in Science).

REFERENCES

[1]T. Erneux, *Applied Delay Differential Equations* (Springer, 2010).
[2]M. Lakshamanan and D. V. Senthikumar, *Dynamics of Nonlinear Time-Delay Systems* (Springer, 2011).
[3]Y. Kuang, *Delay Differential Equations with Applications in Population Dynamics* (Academic Press, Boston, 1993).
[4]J. Li, Y. Kuang, and C. Mason, J. Theor. Biol. **242**, 722–735 (2006).
[5]H. L. Smith, *An Introduction to Delay Differential Equations with Applications to the Life Sciences*, Texts in Applied Mathematics (Springer, New York, 2011).
[6]P. Grindrod and D. Pinotsis, Physica D **240**, 13–20 (2010).
[7]S. Gan, J. Comput. Appl. Math. **206**, 898–907 (2007).
[8]H. Chen and C. Zhang, "Convergence and stability of extended block boundary value methods for Volterra delay integro-differential equations," Appl. Numer. Math. **62**, 141–154 (2012).
[9]M. C. Soriano, J. Garcia-Ojalvo, C. R. Mirasso, and I. Fischer, "Complex photonics: Dynamics and applications of delay-coupled semiconductors lasers," Rev. Mod. Phys. **85**, 421–470 (2013).
[10]L. Larger, "Complexity in electro-optic delay dynamics: Modelling, design and applications," Philos. Trans. R. Soc. A **371**, 20120464 (2013).
[11]X. S. Yao and L. Maleki, "Optoelectronic microwave oscillator," J. Opt. Soc. Am. B **13**, 1725–1735 (1996).
[12]L. Maleki, "The optoelectronic oscillator," Nat. Photonics **5**, 728–730 (2011).
[13]J. Yang, J.-L. Yu, Y.-T. Wang, L.-T. Zhang, and E.-Z. Yang, "An optical domain combined dual-loop optoelectronic oscillator," IEEE Photon. Technol. Lett. **19**, 807–809 (2007).
[14]Y. K. Chembo, L. Larger, R. Bendoula, and P. Colet, "Effects of gain and bandwidth on the multimode behavior of optoelectronic microwave oscillators," Opt. Express **16**, 9067–9072 (2008).
[15]J. M. Kim and D. Cho, "Optoelectronic oscillator stabilized to an intra-loop Fabry-Perot cavity by a dual servo system," Opt. Express **18**, 14905–14912 (2010).
[16]W. Li and J. Yao, "An optically tunable optoelectronic oscillator," IEEE J. Lightw. Technol. **28**, 2640–2645 (2010).
[17]E. C. Levy and M. Horowitz, "Single-cycle radio-frequency pulse generation by an optoelectronic oscillator," Opt. Express **19**, 17599–17608 (2011).
[18]I. Ozdur, M. Akbulut, N. Hoghooghi, D. Mandridis, M. U. Piracha, and P. J. Delfyett, "Optoelectronic loop design with 1000 finesse Fabry–Perot etalon," Opt. Lett. **35**, 799–801 (2010).
[19]O. Okusaga, E. J. Adles, E. C. Levy, W. Zhou, G. M. Carter, C. R. Menyuk, and M. Horowitz, "Spurious mode reduction in dual injection-locked optoelectronic oscillators," Opt. Express **19**, 5839–5854 (2011).
[20]R. M. Nguimdo, Y. K. Chembo, P. Colet, and L. Larger, "On the phase noise performance of nonlinear double-loop optoelectronic microwave oscillators," IEEE J. Quantum Electron. **48**, 1415–1423 (2012).
[21]K. Saleh, R. Henriet, S. Diallo, G. Lin, R. Martinenghi, I. V. Balakireva, P. Salzenstein, A. Coillet, and Y. K. Chembo, "Phase noise performance comparison between optoelectronic oscillators based on optical delay lines and whispering gallery mode resonators," Opt. Express **22**, 32158–32173 (2014).
[22]A. F. Talla, R. Martinenghi, G. R. G. Chengui, J. H. Talla Mbé, K. Saleh, A. Coillet, G. Lin, P. Woafo, and Y. K. Chembo, "Analysis of phase-locking in narrow-band optoelectronic oscillators with intermediate frequency," IEEE J. Quantum Electron. **51**, 5000108 (2015).
[23]A. Argyris, D. Syvridis, L. Larger, V. Annovazzi-Lodi, P. Colet, I. Fischer, J. Garcia-Ojalvo, C. R. Mirasso, L. Pesquera, and K. A. Shore, "Chaos-based communications at high bit rates using commercial fibre-optic links," Nature **438**, 343–346 (2005).
[24]R. M. Nguimdo, R. Lavrov, P. Colet, M. Jacquot, Y. K. Chembo, and L. Larger, "Effect of fiber dispersion on broadband chaos communications implemented by electro-optic nonlinear delay phase dynamics," J. Lightw. Technol. **28**, 2688–2696 (2010).
[25]J. Ai, L. Wang, and J. Wang, "Secure communications of CAP-4 and OOK signals over MMF based on electro-optic chaos," Opt. Lett. **42**, 3662–3665 (2017).
[26]J. Oden, R. Lavrov, Y. K. Chembo, and L. Larger, "Multi-Gbit/s optical phase chaos communications using a time-delayed optoelectronic oscillator with a three-wave interferometer nonlinearity," Chaos **27**, 114311 (2017).
[27]M. Grapinet, V. Udaltsov, M. Jacquot, P.-A. Lacourt, J. M. Dedley, and L. Larger, "Experimental chaotic map generated by picosecond laser pulse-seeded electro-optic nonlinear delay dynamics," Chaos **18**, 013110 (2008).
[28]Y. K. Chembo, "Laser-based optoelectronic generation of narrowband microwave chaos for radars and radio-communication scrambling," Opt. Lett. **42**, 3431–3434 (2017).
[29]L. Larger, A. Baylon-Fuentes, R. Martinenghi, V. S. Udaltsov, Y. K. Chembo, and M. Jacquot, "High-speed photonic reservoir computing using a time-delay-based architecture: Million words per second classification," Phys. Rev. X **7**, 011015 (2017).
[30]X. Zou, X. Liu, W. Li, P. Li, W. Pan, L. Yan, and L. Shao, "Optoelectronic oscillators (OEOs) to sensing, measurement, and detection," IEEE J. Quantum Electron. **52**, 0601116 (2016).
[31]K. Ikeda, "Multiple-valued stationary state and its instability of the transmitted light by a ring cavity system," Opt. Commun. **30**, 257–261 (1979).
[32]Y. C. Kouomou, P. Colet, L. Larger, and N. Gastaud, "Chaotic breathers in delayed electro-optical systems," Phys. Rev. Lett. **95**, 203903 (2005).
[33]A. B. Cohen, B. Ravoori, T. E. Murphy, and R. Roy, "Using synchronization for prediction of high-dimensional chaotic dynamics," Phys. Rev. Lett. **101**, 154102 (2008).
[34]L. Weicker, T. Erneux, O. D'Huys, J. Danckaert, M. Jacquot, Y. K. Chembo, and L. Larger, "Strongly asymmetric square waves in a time-delayed system," Phys. Rev. E **86**, 055201 (2012).
[35]L. Weicker, T. Erneux, O. D'Huys, J. Danckaert, M. Jacquot, Y. K. Chembo, and L. Larger, "Slow-fast dynamics of a time-delayed electro-optic oscillator," Philos. Trans. R. Soc. A **371**, 20120459 (2013).
[36]K. E. Callan, L. Illing, Z. Gao, D. J. Gauthier, and E. Scholl, "Broadband chaos generated by an optoelectronic oscillator," Phys. Rev. Lett. **104**, 113901 (2010).
[37]D. P. Rosin, K. E. Callan, D. J. Gauthier, and E. Scholl, "Pulse-train solutions and excitability in an optoelectronic oscillator," Eur. Phys. Lett. **96**, 34001 (2011).

Published under license by AIP Publishing.

[38]B. Ravoori, A. B. Cohen, J. Sun, A. E. Motter, T. E. Murphy, and R. Roy, "Robustness of optimal synchronization in real networks," Phys. Rev. Lett. **107**, 034102 (2011).
[39]G. R. G. Chengui, A. F. Talla, J. H. Talla Mbé, A. Coillet, K. Saleh, L. Larger, P. Woafo, and Y. K. Chembo, "Theoretical and experimental study of slow-scale Hopf limit-cycles in laser-based wideband optoelectronic oscillators," J. Opt. Soc. Am. B **31**, 2310–2316 (2014).
[40]B. A. Marquez, J. J. Suarez-Vargas, and J. A. Ramírez, "Polynomial law for controlling the generation of n-scroll chaotic attractors in an optoelectronic delayed oscillator," Chaos **24**, 033123 (2014).
[41]J. H. Talla Mbé, A. F. Talla, G. R. G. Chengui, A. Coillet, L. Larger, P. Woafo, and Y. K. Chembo, "Mixed-mode oscillations in slow-fast delayed optoelectronic systems," Phys. Rev. E **91**, 012902 (2015).
[42]Y. K. Chembo, M. Jacquot, J. M. Dudley, and L. Larger, "Ikeda-like chaos on a dynamically filtered supercontinuum light source," Phys. Rev. A **94**, 023847 (2016).
[43]B. Romeira, J. Javaloyes, J. M. L. Figueiredo, C. N. Ironside, H. I. Cantu, and A. E. Kelly, "Delayed feedback dynamics of Lienard-type resonant tunneling-photo-detector optoelectronic oscillators," IEEE J. Quantum Electron. **49**, 31–42 (2013).
[44]Y. A. Kuznetsov, *Elements of Applied Bifurcation Theory*, 2nd ed. (Springer-Verlag, New York, 1998).
[45]J. Guckenheimer and P. Holmes, *Nonlinear Oscillations, Dynamical Systems and Bifurcations of Vectors Fields*, Applied Mathematical Sciences Vol. 42 (Springer, 1985).
[46]M. Haragus and G. Iooss, *Local Bifurcations, Center Manifolds, and Normal Forms in Infinite-Dimensional Dynamical Systems* (Springer, 2010).
[47]M. Han and P. Yei, *Normal Forms, Melnikov Functions and Bifurcation of Limit Cycles* (Springer, 2012).
[48]A. H. Nayfeh, *The Method of Normal Forms* (Wiley-VCH, 2011).
[49]L. Illing and D. J. Gauthier, "Hopf bifurcations in time-delay systems with band-limited feedback," J. Opt. Soc. Am. B **13**, 1725–1735 (1996).
[50]G. R. G. Chengui, P. Woafo, and Y. K. Chembo, "The simplest laser-based optoelectronic oscillator: An experimental and theoretical study," IEEE J. Lightw. Technol. **34**, 873–878 (2016).
[51]G. R. G. Chengui, J. H. Talla Mbé, A. F. Talla, P. Woafo, and Y. K. Chembo, "Dynamics of optoelectronic oscillator with electronic and laser nonlinearity," IEEE J. Quantum Electron. **54**, 5000207 (2018).
[52]B. Ravoori, A. B. Cohen, A. V. Setty, F. Serrentino, T. E. Murphy, E. Ott, and R. Roy, "Adaptive synchronization of coupled chaotic oscillators," Phys. Rev. E **80**, 056205 (2009).

Published under license by AIP Publishing.